

Analysis of Corrugation Pitch Influence on Pressure Distribution and Flow Maldistribution in Chevron-Type Plate Heat Exchangers



Bhupal Kumar^{*}, Bimal Kumar

Hydraulic Laboratory, Government Engineering College, Jamui 811313, India

Corresponding Author Email: kbhupal246@gmail.com

Copyright: ©2024 The authors. This article is published by IIETA and is licensed under the CC BY 4.0 license (<http://creativecommons.org/licenses/by/4.0/>).

<https://doi.org/10.18280/ijht.420429>

ABSTRACT

Received: 11 March 2024

Revised: 16 July 2024

Accepted: 1 August 2024

Available online: 31 August 2024

Keywords:

plate heat exchanger, corrugation pitch, flow maldistribution, channel pressure drop, total non-dimensional pressure drop

The current research analyses the influence of corrugation pitch on channel frictional factor (CFF), channel pressure drops, and total pressure drop in a single pass chevron plate heat exchanger, across Reynolds numbers ranging from 2004 to 5421. Single corrugated chevrons with a chevron angle of 60° are utilized. Corrugation pitch significantly influences fluid flow distribution in the channels, consequently affecting flow maldistribution, and pressure drop in PHEs. Additionally, the enhancement in CFF for decreasing the aspect ratio at the same flow rate is examined. The study reveals a decrease in channel pressure drops in the range of 79.79% to 82.25%, when increasing the corrugation pitch from 12 mm to 30 mm and decreasing the aspect ratio from 56.4 to 31.33. The current analytical results have been confirmed by comparing them with the experimental findings reported in previous studies. Although higher pressure drops can enhance heat transfer by increasing turbulence and improving flow distribution, however they demand more energy for pumping, that can ultimately impact overall system's efficiency. Hence, finding an optimal balance is crucial for achieving efficient heat exchanger operation.

1. INTRODUCTION

Plate heat exchangers (PHEs) play a pivotal role in energy conservation and efficient energy utilization. They are recognized for their notably high area density. The high area density can be described as the ratio of surface area's of heat transfer to the heat exchanger's volume. This characteristic results in a smaller hydraulic diameter for fluid flow that leads to higher efficiency than conventional tubular heat exchangers, all within a much smaller volume. In recent years, PHEs have gained widespread adoption across various industries including heating, cooling, and heat-regeneration. These heat exchangers are chosen for their beneficial features, such as high overall heat transfer rates, enhanced heat transfer coefficients and areas, excellent efficiency, suitability for sanitary applications in industries like brewing, and food production, as well as ease of maintenance.

Mueller and Chiou [1] conducted a thorough review focusing on the challenges associated with maldistribution. Meanwhile, Bassiouny and Martin [2, 3] conducted an in-depth analysis of PHEs, encompassing the derivation of parameters such as axial velocity, total pressure drops, and pressure distributions in the entry and exit ports. They also explored flow distribution within the channels. Their investigation resulted in the establishment of a generalized parameter, designated as m^2 , which represents flow maldistribution. This parameter was formulated by considering mass and momentum equations for both entry and exit port flows across different PHEs. In his research, Bajura

[4] conducted a thorough analysis of flow distribution systems in inlet and exit ports. He created a mathematical framework to elucidate the flow dynamics at specific junctions within the manifold, emphasizing the importance of momentum balance. Acrivos et al. [5] conducted research on the partitioning of fluid streams within manifolds, focusing on pressure alterations caused by wall friction and fluctuations in fluid momentum. Meanwhile, Martin [6] studied the effects of the largest flow path and the interaction between crossings and longitudinal flow. Through his analysis, he derived a simple equation for the friction factor that considers parameters such as the chevron angle and Reynolds number. This equation provides a plausible depiction of the system's behavior. Kumar and Singh [7] studied the hydraulic performance analysis of PHE with a chevron angle of 60°. Yong et al. [8] investigated the PHE's flow characteristics and developed a PHE resistance calculation model.

Mulley and Manglik [9] undertook experimental research focusing on turbulent flow heat transfer and pressure drop within the PHE. Their study investigated various corrugation angles to understand their impact on heat transfer and pressure drop features. They considered equal flow rates in channels for their studies. Tereda et al. [10] studied conduit-to-channel uneven division of fluid flow in PHEs with a fixed number of plates and corrugated angles, while varying port diameters. Gulenoglu et al. [11] conducted experimental research focusing on the thermo-hydraulic performance of three distinct plate. Further, with experimentation they introduced a correlation for novel correlation to describe the relationship

between the Nusselt number and friction factor. This correlation provides a mathematical representation that connects these essential parameters, aiding in the understanding and prediction of heat transfer and fluid flow characteristics within the studied system. Faizal and Ahmed [12] focused on the pressure drop and heat transfer in PHEs with varying spacings between corrugated plates. Han et al. [13] performed numerical simulations and experimental analyses to investigate the temperature, pressure, and velocity fields in corrugated PHEs. Their observations included temperature distributions and pressure reductions along the flow direction. Focke et al. [14] carried out experimental investigations to assess how corrugation inclination angles affect the thermohydraulic performance of PHEs. They assumed uniform flow within each channel. Their study provides insights into the correlation between corrugation angles, heat transfer efficiency, and fluid flow characteristics within these exchangers. Khan et al. [15] studied the effects of heat transfer characteristics in single-phase flow across a range of Reynolds numbers, chevron angles, and corrugation depths. Nilpueng and Wongwises [16] examined heat transfer coefficients and water flow's pressure drops within PHEs featuring rough surfaces, comparing them with smooth surfaces. Bobbili et al. [17] and Rao and Das [18] conducted experimental investigations on flow maldistribution in PHEs, considering various plate's package sizes and corrugation angles. They observed that flow maldistribution increased with overall pressure drop. Fernandes et al. [19] examined flow characteristics in corrugated-type PHEs, different chevron angles, aspect ratios, and fluid viscosities at lower Reynolds numbers. They observed correlations between friction factors, aspect ratios, and chevron angles. Agarwal [20] examined the temperature distribution, effectiveness, and total heat transfer coefficient for various Reynolds numbers in PHEs.

The literature review identifies a significant research gap concerning the impact of corrugation pitch as a crucial parameter in a PHE. Specifically, there is a shortage of comprehensive studies exploring how corrugation pitch influences the channel frictional factor (CFF), flow maldistribution, channel pressure drop, and overall nondimensional pressure drop. The present study aims to fill these gaps.

2. PLATE GEOMETRY

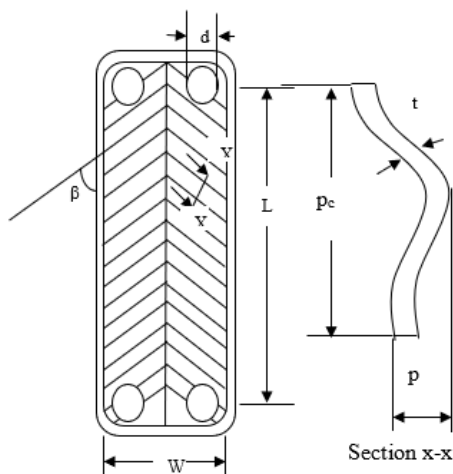


Figure 1. The geometric features of the plate

The thermo-hydraulic performance of PHEs is significantly influenced by several geometric features of chevron plates, as highlighted in the previous studies [9, 10]. The parameters mentioned include the corrugation angle (β), which describes the angle of the corrugations on the plates, and the area enlargement factor (φ). The φ is the ratio of the plate's effective area and the plate's projected area. These parameters are illustrated in Figure 1, which also depicts the plate specifications and a sectional view (x-x).

3. MATHEMATICAL FORMULATION

The plate configuration utilized for analytical computations is presented in Figure 1. These plates, densely packed and featuring sine-wave corrugations, constrain open flow passages intersecting at an angle of β , resulting in a complex flow pattern and temperature distribution. This setup holds promises for achieving high heat transfer rates while maintaining relatively low pressure drops. Analytical studies of sine waves suggest that the length of the curve between two fixed points varies depending on both the amplitude and the period of the wave.

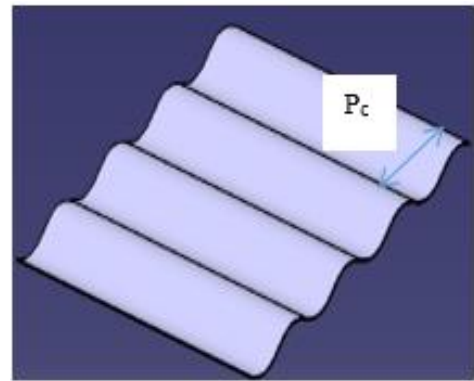


Figure 2. Sinusoidal corrugated plate

For demonstrating the changes in curve length between two fixed points having variations in amplitude and period, the sine waves geometry is shown in Figure 2. The plate's geometry resembles a sinusoidal curve, enabling the expression of the corresponding sine wave equation as shown in Figure 3.

$$y = \frac{p}{2} \sin \frac{2\pi}{p_c} x \quad (1)$$

The length of the curve described by the equation $\{y=f(x), z=0\}$ between $x=a$ and $x=b$ is given by:

$$L_\lambda = \int_a^b \sqrt{1 + y'^2} dx \quad (2)$$

The chevron pattern's wavelength aligns with the corrugated pitch, as depicted in Figure 1. In this representation, the sinusoidal corrugation's amplitude is labeled as p , while the plate thickness is denoted as t . Considering the sinusoidal curve of the wavy surfaces, the length of a sine curve can be expressed as:

$$L_\lambda = \int_0^{p_c} \sqrt{1 + \left(\frac{\pi p}{p_c}\right)^2 \cos^2\left(\frac{2\pi x}{p_c}\right)} dx \quad (3)$$

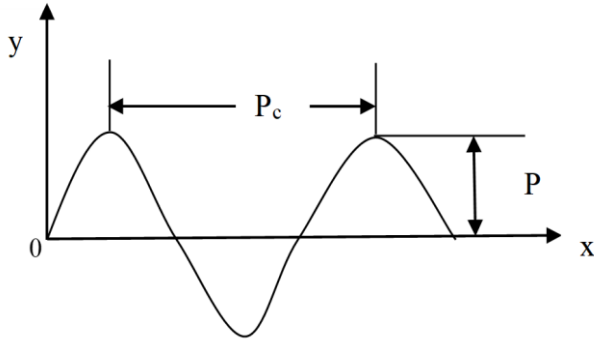


Figure 3. Sine curve for plate geometry

Eq. (3) represents an elliptical integral, and therefore, its solution can be obtained as follows:

$$L_{\lambda} = \int_0^{p_c} \sqrt{1 + \left(\frac{\pi p}{p_c}\right) \cos^2\left(\frac{2\pi x}{p_c}\right)} dx = \frac{\sqrt{\frac{\pi p}{p_c} + 1}}{\frac{2\pi}{p_c}} E\left[\frac{\frac{\pi p}{p_c}}{\left(\frac{\pi p}{p_c} + 1\right)}\right] \quad (4)$$

The incomplete elliptical integral solution of the second kind is provided by Brown [21].

$$E\left(\frac{\phi}{m}\right) = \int_0^{\phi} (1 - m \sin^2 \theta)^{\frac{1}{2}} d\theta \\ = \frac{2\phi}{\pi} E + \sin \phi \cos \phi \left[\frac{1}{2} A_2 m\right. \\ \left. + \frac{1}{2 * 4} A_4 m^2 + \frac{1 * 3}{2 * 4 * 6} A_6 m^3\right. \\ \left. + \dots\right] \quad (5)$$

where, $A_2 = \frac{1}{2}$, $A_4 = \frac{3}{2 * 4} + \frac{1}{4} \sin^2 \phi$, $A_6 = \frac{3 * 5}{2 * 4 * 6} \sin^2 \phi + \frac{1}{6} \sin^2 \phi$ and $E = 1 + \frac{1}{2} \left\{ \ln \left[4(1 - m)^{\frac{-1}{2}} \right] - \frac{1}{1.2} \right\} (1 - m) + \frac{1^2 * 3}{2^2 * 4} \left\{ \ln \left[4(1 - m)^{\frac{-1}{2}} \right] - \frac{2}{1.2} - \frac{1}{3 * 4} \right\} (1 - m)^2 + \frac{1^2 * 3^2 * 5}{2^2 * 4^2 * 6} \left\{ \ln \left[4(1 - m)^{\frac{-1}{2}} \right] - \frac{2}{1.2} - \frac{2}{3 * 4} - \frac{1}{5 * 6} \right\} (1 - m)^3 + \dots$

The enlargement factor (φ) can be expressed as:

$$\varphi = \frac{L_{\lambda}}{p_c} \int_0^{p_c} \sqrt{1 + \left(\frac{2\pi p}{p_c}\right) \cos^2\left(\frac{2\pi x}{p_c}\right)} dx \quad (6)$$

The surface enlargement factor for sinusoidal corrugation can be approximately determined using the following method:

$$\varphi \approx \frac{1}{6} \left\{ 1 + \sqrt{1 + x^2} + 4 \sqrt{1 + \frac{x^2}{2}} \right\} \quad (7)$$

where, $x = \frac{\pi p}{p_c}$.

It is crucial to emphasize that the Reynolds number for a PHE is expressed in terms of D_h (hydraulic diameter) which can be expressed as follows:

$$Re = \frac{u_{ch}}{v} (D_h) \quad (8)$$

$D_h = 2bLw/(b+Lw)$ φ Since $b < Lw$, $D_h = 2b/\varphi$.

The fluid mean velocity in the channel can be expressed as:

$$u_{ch} = \frac{V}{wbn} \quad (9)$$

Martin [6] provided one of the correlations for the friction factors of PHEs with chevron patterns. The Fanning friction factor can be expressed as:

$$f = \left[\frac{\cos \beta}{\left(0.045 \tan \beta + 0.09 \sin \beta + \frac{f_o}{\cos \beta} \right)^{\frac{1}{2}} + \frac{1 - \cos \beta}{\sqrt{3.8 f_1}} } \right]^{-0.5} \quad (10)$$

where, $f_o = \frac{16}{Re}$ for $Re < 2000$ and $f_o = (1.56 \ln Re - 3.0)^{-2}$ for $Re > 2000$ $f_1 = \frac{149.25}{Re} + 0.9625$ for $Re < 2000$ and $f_1 = \frac{9.75}{Re^{0.289}}$ for $Re > 2000$.

To validate the analytical results, the friction factor correlation for the existing PHE was compared with experimental data [18].

$$f = 21.41 Re^{-0.301} \quad (11)$$

The total pressure drop, comprising the channel's pressure drop, port's pressure drop, (with an inner diameter of 25.4 mm), and the pressure drop in the passages, can be calculated using the following equation:

$$\Delta P_{tp} = \Delta P_{cm} + \Delta P_{port} + \Delta P_{ec} \quad (12)$$

The calculation of the port's pressure drop relies on the total flow rate and is determined by empirically established equation [17].

$$\Delta P_{port} = 1.5 \rho \frac{V^2 p}{2} \quad (13)$$

The pressure drops attributed to bends, sudden contractions, and sudden expansions at the entry and exits are determined using the following formula:

$$\Delta P_{ec} = K_{ec} \rho \frac{V^2 p}{2} \quad (14)$$

where, K_{ec} represents the total pressure loss coefficient associated with bends, sudden contractions, and sudden expansions at the entry and exit of the conduits.

The pressure drops resulting from friction in the corrugated passage are evaluated from flow rate, employing an empirical formula.

$$\Delta P_{chm} = f_{ch} \frac{L_{ch}}{d_h} \rho \frac{V_{ch}^2}{2} \quad (15)$$

The value of m^2 is determined using the equation provided by Bassiouny and Martin [2] for similar entry and exit port dimensions (Details are given in the Appendix).

$$m^2 = \left(\frac{n A_c}{A_p} \right)^2 \frac{1}{\xi_c} \quad (16)$$

Here, ξ_c represents the total frictional resistance of the channel and is equal to $\xi_c = f L_{ch}/d_h$ plus other minor losses.

The total nondimensional pressure drop of the PHE is calculated as:

$$p_{in} - p_o = \left(\frac{m^2}{\tanh^2 m} \right) \left(\frac{A_p}{nA_c} \right)^2 \frac{\xi_c}{2} \quad (17)$$

The variation in pressure drop from the first to the last channel is determined using an equation from Bassiouny and Martin [2], which is based on the flow maldistribution parameter (m^2).

$$\frac{\Delta P}{\rho W_o^2} = \left(\frac{A_p}{nA_c} \right)^2 \frac{\xi_c}{2} m^2 \frac{(\cosh m(1-z))^2}{(\sinh m)^2} \quad (18)$$

4. RESULTS AND DISCUSSION

Tables 1 and 2 present the geometric features of a chevron plate and the scope of operational parameters examined in the current investigation, respectively.

Table 1 demonstrates the range of parameters under consideration in this research. Building upon these observations, the current research endeavors to analytically explore the m^2 alongside the pressure drop in PHEs across a diverse spectrum of Reynolds numbers, corrugation pitches, and channel aspect ratios.

Table 1. Description of the geometrical characteristics of a chevron plate considered in the present study

Sl. No	Terminology	Parameters
1.	Length of plate, L	726 mm
2.	Width of plate, W	141 mm
3.	Corrugation pitch	12 mm
4.	Amplitude of plate	2.38 mm
5.	Plate thickness, t	0.5 mm
6.	Chevron angle	$\beta = 60^\circ$
7.	Number of channels per fluid	8-7

Table 2. The operational parameters considered in the present study span the following ranges

Sl. No	Terminology	Parameters Range
1.	Corrugation pitch (mm)	$P_c = 12 - 30$
2.	Reynolds number	$Re = 2004 - 5421$
3.	Channel aspect ratio	$A = 56.4 - 31.33$
4.	Maldistribution parameter, m^2	$m^2 = 0.99 - 6.33$
5.	Flow rate (L/sec)	$0.139 - 5.55$

4.1 Validation

4.1.1 Confirmation with experimental results conducted by Rao and Das [18]

In Figure 4, a comparison is made between the analytical results of the CFF obtained in this study and the experimental data from Rao and Das [18]. The sets of results show strong agreement, with discrepancies within 5%. From Figure 4, it is clear that the CFF decreases as the channel Reynolds number increases. It happens due to the concurrent rise in channel velocity for a fixed number of channels.

4.2 Typical results

4.2.1 Exploring CFF in relation to corrugation pitch

Figure 5 explored the CFF with corrugation pitch is

illustrated for a fixed channel aspect ratio and flow rate in the PHE. It is clear from Figure 5 that the CFF decreases as the corrugation pitch increases. Additionally, it is observed that the loss friction factor for higher channel aspect ratio values is smaller compared to that of smaller channel aspect ratio values, for the same rate of water flow in the PHE. This phenomenon is attributed to the increased channel flow velocity in channels with higher aspect ratios.

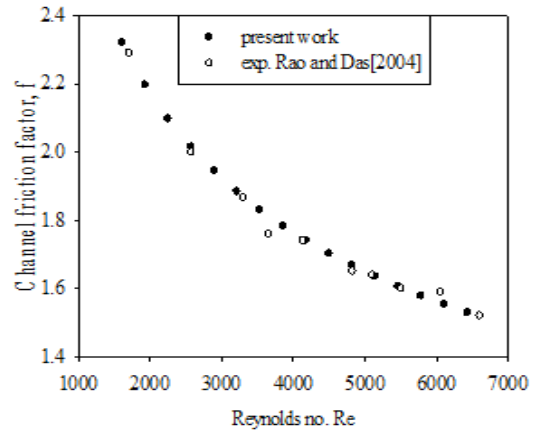


Figure 4. Exploring CFF in relation to Reynolds number

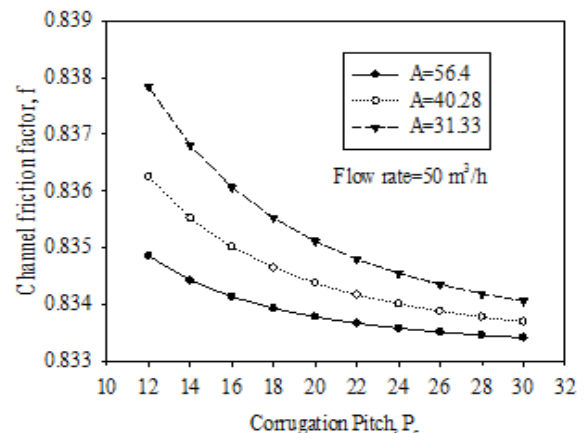


Figure 5. Exploring CFF in relation to corrugation pitch

At lower corrugation pitches, momentum dominates over viscous forces, leading to a slower increase in the velocity gradient. Moreover, reduced corrugation pitches encourage swirling fluid movement within the inter-plate channels, leading to increased friction within the channels. It is important to highlight that the friction factor decreases at a declining rate as the corrugation pitch increases, primarily due to the heightened pressure drop penalty associated with lower aspect ratios.

4.2.2 Exploring CFF in relation to Reynolds number

Figure 6 depicts the exploring CFF with Reynolds number for various corrugation pitches and a fixed channel aspect ratio. The trend depicted in Figure 6 indicates that the CFF decreases with increasing Reynolds number. Additionally, it's observed that the loss friction factor for smaller channel aspect ratio values is greater compared to that of larger channel aspect ratio values for the equal rate of water flow in the PHE. Another contributing factor to this behavior may be the change in the flow regime within the PHE as the hydraulic diameter

increases and the enlargement factor decreases.

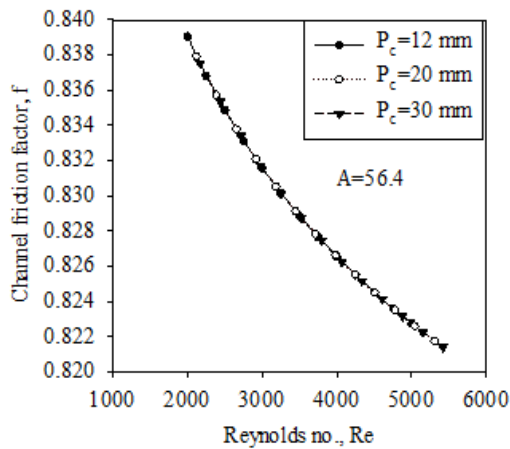


Figure 6. Exploring CFF in relation to Reynolds number and corrugation pitches

4.2.3 Exploring channel pressure drop in relation to corrugation pitch

Figure 7 illustrates the exploring pressure drop in the channel with corrugation pitch for three different aspect ratios and a fixed flow rate in the PHE. It is noted that with the increase in the corrugation pitch of the plate, the pressure drops decrease across all aspect ratios. This suggests that a larger corrugation pitch facilitates a smoother flow, reducing resistance and thus the pressure drop. The pressure drop is highest at the maximum aspect ratio. This is likely due to the increased flow disturbances caused by the more complex flow path in channels with higher aspect ratios. The disturbances can increase friction and turbulence, leading to a greater pressure drop.

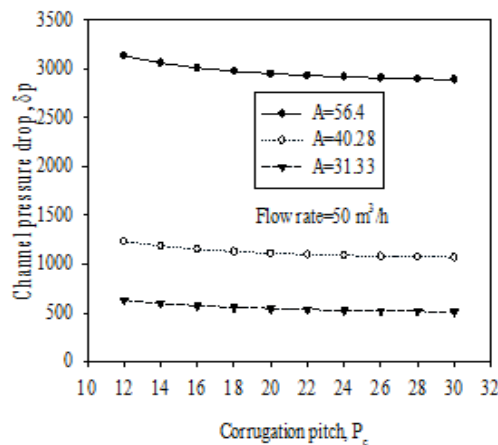


Figure 7. Exploring pressure drop in channel in relation to corrugation pitch

4.2.4 Exploring channel pressure drop in relation to Reynolds number

Figure 8 depicts the exploring pressure drop in the channel in relation to Reynolds number for three different corrugation pitches and a fixed channel aspect ratio. The analysis shows that the pressure drop rises as the Reynolds number increases for all corrugation pitch values. Additionally, the channel pressure drop reaches its peak at the lowest corrugation pitch value due to the higher value of the enlargement factor,

resulting in a reduced hydraulic diameter of the PHE. Higher pressure drops can lead to better flow distribution throughout the PHE, promoting more uniform movement of fluid through the channels. This improved flow uniformity enhances heat transfer efficiency by ensuring more effective contact between the fluid and the surface area of the PHE.

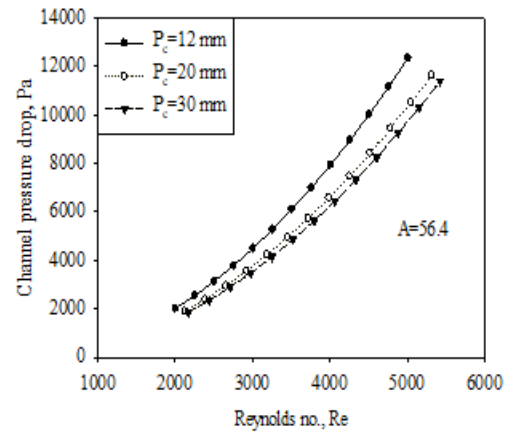


Figure 8. Exploring pressure drop in channel in relation to Reynolds number

4.2.5 Exploring flow maldistribution parameter in relation to corrugation pitch

Figure 9 illustrates the exploration of the, m^2 with corrugation pitch for varying channel aspect ratios and a fixed flow rate in a U-type PHE. At higher channel aspect ratio values, minimal variation is observed in the m^2 value with corrugation pitch. As depicted in Figure 9, the, m^2 , increases with a decrease in channel aspect ratio for the same corrugation pitch and water flow rate in the U-type PHE. This trend arises from the fact that m^2 is influenced by channel velocity, where a larger m^2 value indicates non-uniform flow within the channel.

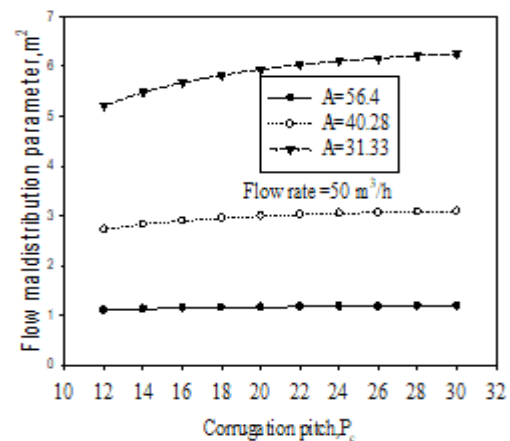


Figure 9. Exploring flow maldistribution parameter in relation to corrugation pitch

4.2.6 Exploring flow maldistribution parameter in relation to Reynolds number

Figure 10 displays the relationship between the m^2 , and the Reynolds number across three distinct corrugation pitches while maintaining a constant channel aspect ratio within a U-type PHE. The observation gleaned from Figure 10 indicates that the flow maldistribution, denoted by m^2 , exhibits an upward trend with increasing corrugation pitch and Reynolds

number, under the condition of a fixed channel aspect ratio and consistent water flow rate in the U-type PHE. This observed trend can be attributed to the fact that maldistribution is greatly influenced by the hydraulic diameter, which experiences variations with changes in corrugation pitch and Reynolds number.

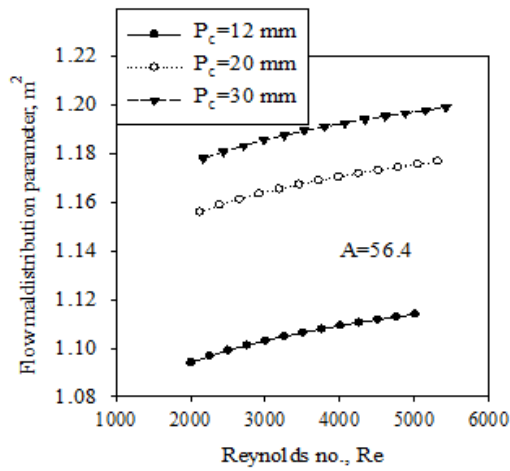


Figure 10. Exploring flow maldistribution parameter in relation to Reynolds number

4.2.7 Exploring total non-dimensional pressure drop in relation to corrugation pitch

Figure 11 depicts a comparison of the total non-dimensional pressure drop across various corrugation pitches for different channel aspect ratios, while maintaining a fixed flow rate in a PHE. From Figure 11, it is clear that the non-dimensional pressure drop decreases as the corrugation pitch increases, irrespective of the channel aspect ratio. This reduction in pressure drop with increasing corrugation pitch can be attributed to the higher channel velocity associated with larger corrugation pitches. Furthermore, the observations from Figure 11 indicate that the pressure drop tends to increase with higher aspect ratios. This increase in pressure drop as the aspect ratio rises is attributed to the reduction in hydraulic diameter, which leads to heightened flow resistance within the channels.

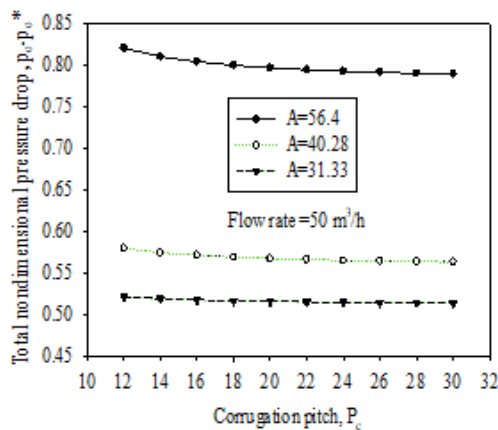


Figure 11. Exploring total non-dimensional pressure drop in relation to corrugation pitch

In summary, the trends observed in Figure 11 underscore the significant impact of corrugation pitch and channel aspect ratio on the non-dimensional pressure drop in U-type PHEs.

Increases in corrugation pitch enhance channel velocity, thereby reducing pressure drop, whereas increases in aspect ratio decrease hydraulic diameter, resulting in heightened pressure drop.

4.2.8 Exploring total pressure drop in relation to Reynolds number

Figure 12 illustrates the exploring in the channel's pressure drop with Reynolds number across various channel aspect ratios and corrugation pitches. From the data presented in Figure 12, it is apparent that the pressure drop increases with rising Reynolds number, regardless of the channel aspect ratios and corrugation pitches. This observed increase in pressure drop with Reynolds number can be attributed to the influence of maldistribution, which is intricately linked to the overall friction coefficient of the corrugated channel and the channel aspect ratios. Moreover, it is noteworthy that the pressure drop tends to decrease as the channel aspect ratio decreases, given a fixed corrugation pitch and consistent flow rate in the PHE. This phenomenon occurs because a reduction in the channel aspect ratio leads to a decrease in the hydraulic diameter, which in turn lowers the overall flow resistance within the channels, resulting in a decreased pressure drop.

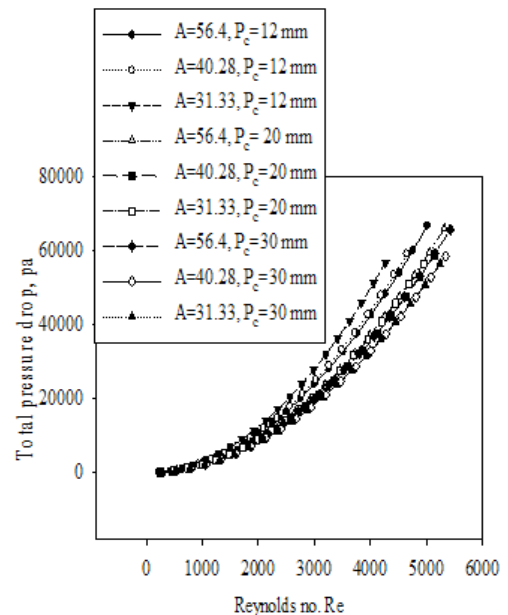


Figure 12. Exploring total pressure drop in relation to Reynolds number

In summary, the trends observed in Figure 12 underscore the complex interplay between Reynolds number, channel aspect ratios, and corrugation pitches in influencing pressure drop in PHEs. Increases in Reynolds number generally lead to heightened pressure drop, while decreases in channel aspect ratio tend to reduce pressure drop due to associated changes in hydraulic diameter and flow resistance.

5. CONCLUSIONS

The analytical presentation of flow maldistribution, and pressure drop considers a broad range of corrugation pitch, Reynolds number, and aspect ratio. The study investigates the effects of corrugation pitch and Reynolds number on CFF, flow maldistribution and channel pressure drop in PHEs. It is

observed that corrugation pitch has an increasing effect on the hydraulic performance of a PHE, with higher aspect ratios leading to larger pressure drops. However, a larger corrugation pitch tends to decrease the channel pressure drop. The analysis reveals that pressure drop increases with the rise in Reynolds number for all corrugation pitch values. Additionally, the flow maldistribution parameter increases with a decrease in channel aspect ratio for the same corrugation pitch and the flow rate in a PHE. Furthermore, it is found that flow maldistribution parameter increases with increasing corrugation pitch and Reynolds number, while maintaining a fixed channel aspect ratio and water flow rate in the PHE. The nondimensional pressure drop decreases with increasing corrugation pitch for three different channel aspect ratios.

It is noted that for a given channel aspect ratio, increasing water flow rate leads to decreased pressure drops in the channels but increases the uneven fluid flow in the channel. Overall, the study highlights the need to balance Reynolds number, corrugation pitch, and aspect ratio to optimize heat exchanger performance.

REFERENCES

- [1] Mueller, A.C., Chiou, J.P. (1988). Review of various types of flow maldistribution in heat exchangers. *Heat Transfer Engineering*, 9(2): 36-50. <https://doi.org/10.1080/01457638808939664>
- [2] Bassiouny, M.K., Martin, H. (1984). Flow distribution and pressure drop in plate heat exchangers—I U-type arrangement. *Chemical Engineering Science*, 39(4): 693-700. [https://doi.org/10.1016/0009-2509\(84\)80176-1](https://doi.org/10.1016/0009-2509(84)80176-1)
- [3] Bassiouny, M.K., Martin, H. (1984). Flow distribution and pressure drop in plate heat exchangers—II Z-type arrangement. *Chemical Engineering Science*, 39(4): 701-704. [https://doi.org/10.1016/0009-2509\(84\)80177-3](https://doi.org/10.1016/0009-2509(84)80177-3)
- [4] Bajura, R.A. (1971). A model for flow distribution in manifolds. *Journal of Engineering for Power*, 93(1): 7-12. <https://doi.org/10.1115/1.3445410>
- [5] Acrivos, A., Babcock, B.D., Pigford, R.L. (1959). Flow distributions in manifolds. *Chemical Engineering Science*, 10(1-2): 112-124. [https://doi.org/10.1016/0009-2509\(59\)80030-0](https://doi.org/10.1016/0009-2509(59)80030-0)
- [6] Martin, H. (1996). A theoretical approach to predict the performance of chevron-type plate heat exchangers. *Chemical Engineering and Processing: Process Intensification*, 35(4): 301-310. [https://doi.org/10.1016/0255-2701\(95\)04129-X](https://doi.org/10.1016/0255-2701(95)04129-X)
- [7] Kumar, B., Singh, S.N. (2015). Analytical studies on the hydraulic performance of chevron type plate heat exchanger. *International Journal of Heat and Technology*, 33(1): 17-24. <https://doi.org/10.18280/ijht.330103>
- [8] Yong, S., Jiayu, R., Yanan, T., Yanxu, N., Menghao, Z. (2018). Research on resistance features of plate heat exchanger based on flow distribution. *International Journal of Heat and Technology*, 36(1): 261-266. <https://doi.org/10.18280/ijht.360135>
- [9] Muley, A., Manglik, R.M. (1999). Experimental study of turbulent flow heat transfer and pressure drop in plate heat exchanger with chevron plates. *ASME Journal of Heat Transfer*, 121(1): 110-117. <https://doi.org/10.1115/1.2825923>
- [10] Tereda, F.A., Srihari, N., Sunden, B., Das, S.K. (2007). Experimental investigation on port-to-channel flow maldistribution in plate heat exchangers. *Heat Transfer Engineering*, 28(5): 435-443. <https://doi.org/10.1080/01457630601163769>
- [11] Gulenoglu, C., Akturk, F., Aradag, S., Uzol, N.S., Kakac, S. (2014). Experimental comparison of performances of three different plates for gasketed plate heat exchangers. *International Journal of Thermal Sciences*, 75: 249-256. <https://doi.org/10.1016/j.ijthermalsci.2013.06.012>
- [12] Faizal, M., Ahmed, M.R. (2012). Experimental studies on a corrugated plate heat exchanger for small temperature difference applications. *Experimental Thermal and Fluid Science*, 36: 242-248. <https://doi.org/10.1016/j.expthermflusci.2011.09.019>
- [13] Han, X.H., Cui, L.Q., Chen, S.J., Chen, G.M., Wang, Q. (2010). A numerical and experimental study of chevron, corrugated-plate heat exchangers. *International Communications in Heat and Mass Transfer*, 37(8): 1008-1014. <https://doi.org/10.1016/j.icheatmasstransfer.2010.06.026>
- [14] Focke, W.W., Zachariades, J., Olivier, I. (1985). The effect of the corrugation inclination angle on the thermohydraulic performance of plate heat exchangers. *International Journal of Heat and Mass Transfer*, 28(8): 1469-1479. [https://doi.org/10.1016/0017-9310\(85\)90249-2](https://doi.org/10.1016/0017-9310(85)90249-2)
- [15] Khan, T.S., Khan, M.S., Chyu, M.C., Ayub, Z.H. (2010). Experimental investigation of single phase convective heat transfer coefficient in a corrugated plate heat exchanger for multiple plate configurations. *Applied Thermal Engineering*, 30(8-9): 1058-1065. <https://doi.org/10.1016/j.applthermaleng.2010.01.021>
- [16] Nilpueng, K., Wongwises, S. (2015). Experimental study of single-phase heat transfer and pressure drop inside a plate heat exchanger with a rough surface. *Experimental Thermal and Fluid Science*, 68: 268-275. <https://doi.org/10.1016/j.expthermflusci.2015.04.009>
- [17] Bobbili, P.R., Sunden, B., Das, S.K. (2006). An experimental investigation of the port flow maldistribution in small and large plate package heat exchangers. *Applied Thermal Engineering*, 26(16): 1919-1926. <https://doi.org/10.1016/j.applthermaleng.2006.01.015>
- [18] Rao, B.P., Das, S.K. (2004). An experimental study on the influence of flow maldistribution on the pressure drop across a plate heat exchanger. *Journal of Fluids Engineering*, 126(4): 680-691. <https://doi.org/10.1115/1.1779664>
- [19] Fernandes, C.S., Dias, R.P., Nóbrega, J.M., Maia, J.M. (2007). Laminar flow in chevron-type plate heat exchangers: CFD analysis of tortuosity, shape factor and friction factor. *Chemical Engineering and Processing: Process Intensification*, 46(9): 825-833. <https://doi.org/10.1016/j.cep.2007.05.011>
- [20] Agarwal, A. (2021). Modelling & numerical investigation of the effectiveness of plate heat exchanger for cooling engine oil using ANSYS CFX. *International Journal of Heat and Technology*, 39(2): 653-658. <https://doi.org/10.18280/ijht.390237>
- [21] Brown, L., Terry. (1970). A Subroutine for the Calculation of The Incomplete Elliptic Integrals of the First and Second Type.

NOMENCLATURE

A	aspect ratio, (L/b)
A _{in}	cross-sectional area of inlet port, m ²
A _o	cross-sectional area of outlet port, m ²
A _p	cross-sectional area of the identical both port, m ²
A _c	cross-sectional area of the channel, m ²
b	plate spacing, m
D _h	hydraulic diameter of the corrugated channel, m
d _{pipe}	connection pipe diameter, m
E	complete elliptical integral of second kind
f	Fanning friction factor
f _{ch}	CFF
k _{ec}	coefficient of total pressure loss
L	vertical distance between the two ports, m
m ²	flow maldistribution parameter
n	number of channels per fluid
p _c	corrugation pitch, m
p	sinusoidal corrugation
P _{in}	inlet port pressure, pa
P _o	outlet port pressure, pa
Δp _{chm}	mean channel pressure drop, pa
Δp _{ec}	pressure drop (sudden expansion and contraction), pa
Δp _{first}	pressure drop at the first channel, pa
Δp _{port}	pressure drop (between the inlet and outlet ports in PHE)
Δp	dimensionless pressure drop across a PHE
Re	Reynolds number, Re=(ρu _c D _h)/μ
t	thickness of plate, m
u _c	dimensionless channel velocity
W	width of the plate, m

Greek letters

β	corrugation angle of the plate (°)
β _{in}	average velocity ratio in the inlet port (=average inlet channel velocity/ inlet port velocity)
β _o	average velocity ratio in the outlet port (=average outlet channel velocity/ outlet port velocity)
φ	area enlargement factor
ρ	density of the fluid, kg/m ³
ξ _c	overall friction coefficient of the corrugated channel

APPENDIX

The flow arrangement of the U-type PHE, including its geometrical and flow path details, is illustrated in Figure 1A.

The analytical solution of differential equations related to flow in ports, can be expressed as follows.

$$\frac{1}{\rho} \frac{d(P_{in} - P_o)}{dZ} + \frac{1}{2} \left[\frac{f_{in}}{D_{in}} + \frac{f_o}{D_o} \left(\frac{A_{in}}{A_o} \right)^2 \right] W^2 - [(2 - \beta_o) \left(\frac{A_{in}}{A_o} \right)^2 - (2 - \beta_{in})] W \frac{dW}{dZ} = 0 \quad (A1)$$

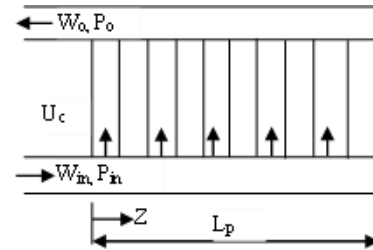


Figure 1A. Flow arrangement for U type plate heat exchanger

The friction loss in the conduits of a plate heat exchanger is considered to be minimal compared to the friction losses within the channels between the plates and the momentum changes caused by flow branching. As a result, Eq. (A1) simplifies to:

$$\frac{1}{\rho} \frac{d(P_{in} - P_o)}{dZ} - [(2 - \beta_o) \left(\frac{A_{in}}{A_o} \right)^2 - (2 - \beta_{in})] W \frac{dW}{dZ} = 0 \quad (A2)$$

The relation between the pressure drop in the channels and the channel velocity can be written in the following form:

$$P_{in} - P_o = \zeta_c \rho \frac{U_c^2}{2} \quad (A3)$$

where, $\zeta_c = 1 + C + f_c \frac{l_c}{d_c} + C^*$ and $U_c = -\frac{A_{in} L}{A_c n} \frac{dW}{dZ}$.

Eqs. (A2) and (A3) can be reduced to dimensionless form after introducing the following dimensionless groups;

$$p = \frac{P}{\rho W_o^2}, \quad w = \frac{W}{W_o}, \quad u_c = \frac{U_c}{W_o}, \quad z = \frac{Z}{L_p}$$

The resulting equations will be given as follows:

$$\frac{d(p_{in} - p_o)}{dz} - [(2 - \beta_o) \left(\frac{A}{A^*} \right)^2 - (2 - \beta_{in})] w \frac{dw}{dz} = 0 \quad (A4)$$

$$p_{in} - p_o = \frac{1}{2} \zeta_c \left(\frac{A}{A_c n} \right)^2 \left(\frac{dw}{dz} \right)^2 \quad (A5)$$

After substituting Eq. (A5) into (A4), one obtains two ordinary differential equations for the velocity in the intake conduit:

$$\frac{d^2 w}{dz^2} - m^2 w = 0 \quad (A6)$$

$$\frac{dw}{dz} = 0 \quad (A7)$$

where, $m^2 = \left[\left(\frac{2 - \beta_o}{2 - \beta_{in}} \right) \left(\frac{A_{in}}{A_o} \right)^2 - 1 \right] \frac{2 - \beta_{in}}{\zeta_c} \left(\frac{n A_c}{A_{in}} \right)^2$.

The value of m^2 is determined using the equation provided by Bassiouny and Martin [2] for similar entry and exit port dimensions.

$$m^2 = \left(\frac{n A_c}{A_p} \right)^2 \frac{1}{\xi_c} \quad (A8)$$

Eq. (A7) represents a case of no fluid flow between the PHE. The boundary conditions applied to Eq. (A6) are $w=1$, at $z=0$

and $w=0$, at $z=1$, the solution of this equation depends on the sign of m^2 , therefore three cases can be taken into consideration but the value of m^2 is positive taken in present analysis.

m^2 is positive, then $\left(\frac{2-\beta_0}{2-\beta_{in}}\right)\left(\frac{A_{in}}{A_0}\right)^2 > 1$, the general solution will take the form.

$$w = C_1 e^{mz} + C_2 e^{-mz} \tag{A9}$$

Applying the foregoing boundary conditions to determine the constants C_1 and C_2 the following are obtained.

The distribution of pressure drop from the initial to the final

channel is determined using the Eq. (A5), which relies on the flow maldistribution parameter, m^2 .

$$\frac{\Delta P}{\rho W_o^2} = \left(\frac{A_p}{nA_c}\right)^2 \frac{\xi_c}{2} m^2 \frac{(\cosh m(1-z))^2}{(\sinh m)^2} \tag{A10}$$

The total nondimensional pressure drop of the PHE. At $z=0$, Eq. (A10) becomes:

$$p_{in} - p_0 = \left(\frac{m^2}{\tanh^2 m}\right) \left(\frac{A_p}{nA_c}\right)^2 \frac{\xi_c}{2} \tag{A11}$$